Supplement to *Infrared-absorbing carbonaceous tar can dominate light absorption by marine-engine exhaust* by J. C. Corbin et al.

Summary of supplementary information

This section contains

- an explicit discussion of the inputs to Figure 1,
- additional methodological discussion,
- a discussion of the analysis which confirmed the absence of char in our SEM images,
- a discussion of the positive artifact in EC for HFO-PM and for asphaltenes,
- a discussion of the measured absorption of unburnt HFO as a function of concentration,
- a discussion of the implication of this manuscript on the interpretation of previous HFO-PM results,
- supplementary figures that were referred to in the main text.

1 Supplementary Discussion

Inputs to Figure 1

The data in Figure 1 reflect literature cited in the main manuscript, model calculations performed in this work, or measurements performed in this work. For clarity, we explicitly describe these details here, where not already specified in the main text. In general, the results from the present work in Figure 1 are the MAE rows (except soot BC and soluble BC), the AAE rows (except soluble brC), the tar brC column (with AAE ranges expanded to accommodate literature data), and the vapourization temperature of tar brC.

Citations are explicitly given in the manuscript for the LAC category, solubility, light absorption, chemical state, carbon bonding, production mechanism, and morphology of all four LAC types (rows 1–5 and 6–7). These rows will not be discussed here.

Vapourization temperature. The vapourization temperature of BC is $\sim 4000\,\mathrm{K}$[1–3]. For tar brC, we have inferred the vapourization temperature as $> 1000\,\mathrm{K}$ because tar brC did not vapourize at 873 K in the HR-AMS (rapid heating) nor at 823 K in the TOA instrument (slow heating). Because tar brC absorbs infrared light but was not detected by SP2, it does not reach incandescence temperatures ($\sim 3000\,\mathrm{K}$) before vapourizing. Therefore, we estimated its vapourization temperature as $\sim 1000\,\mathrm{K}$. The vapourization temperature of soluble brC is given as $< 600\,\mathrm{K}$ since thermal denuding at such temperatures has been successfully employed to remove it from PM samples[4–6].

Size. The typical size of soot BC has been discussed in Bond et al.[3] Our reported range of 0.02 to 0.2 μm may represent, for example, aviation turbines at the lower limit[7] and wood combustion at the upper limit[8]. The typical size of char BC has been discussed in the literature[9–12]. The typical size given for tar brC summarizes the data of Chakrabarty et al.[13] and Alexander et al.[14]. The typical size given for soluble brC represents typical Aitken or accumulation-mode particles in the atmosphere[15].

MAEs. The MAEs given for soot-BC are those of Bond et al.[16], scaled using an AAE of 1.0. The MAEs given for char BC were calculated using the core-shell model described in Methods, for the particle size range specified in the figure, 1–5 μm; these char MAEs are all similar as they are largely controlled by the large diameters rather than the wavelength. The MAEs given for tar brC includes the lower limit of our study (mean minus 1σ) and the upper limit given by Alexander et al.[14] The MAEs given for soluble brC represent the wide range of values reported in the literature.[6,17–19] (We note that Moschos et al. included studies such as Alexander et al.[14] in their summary of brC studies, which represent tar brC rather than soluble brC; we also note that Kumar et al. provide MAEs for both optically-defined brC and soluble brC.)

AAEs. The AAEs given for soot-BC represent the range we calculated using the exact results of the numerical model described in the manuscript. These AAEs were constant as a function of wavelength (since our model used a constant refractive index) and were validated by our measurements (Figure 5). The model yielded AAE(370,950) from 1.04 to 1.10 and AAE(880,950) from 1.03 to 1.21 (see Supplementary Figure 9 for size dependence). While these AAEs are all greater than unity, Scarnato et al.[20] showed that more-compact aggregates can have AAEs as low as 0.8. We therefore reported the lower AAE range for soot-BC as 0.8 in Figure 1.

The AAEs given for char-BC represent the output of the core-shell cenosphere model described in Methods, which is shown in Supplementary Figure 9. The range of values given reflects the output of that model for particles of 0.5–3.0 μm outer diameter, a range which represents the supermicron mode expected for char BC.

The AAEs given for tar brC represent the range of values observed in our work, by Alexander et al.[14], by Chakrabarty et al.[13], and by Hoffer et al.[21]. These data are shown in Figure 5 and were represented as spheres of diameter 100 nm.

The AAEs given for soluble brC represent the range of AAEs reported in the literature[18,22,23], for the wavelengths at which soluble-brC absorption is substantial. Although AAEs up to slightly larger than our upper limit have been reported, the imaginary refractive index also tends to zero as the AAE increases. We therefore truncated the range of reported values to represent this fact. Note that, although we did measure soluble brC AAE(λ, 950) for asphaltenes in HFO, reporting those AAEs in Figure 1 would only confuse the reader, since asphaltenes are not atmospherically relevant. We have introduced the phrase "soluble brC" to describe the material reported in conventional solvent-extraction-based studies of atmospheric brC.

Aerosol mass spectrometry

We employed an Aerodyne High-Resolution Aerosol Mass Spectrometer (HR-AMS) equipped with a switchable 1064 nm soot-vapourization laser to investigate the refractory nature of tar. We refer to the data acquired with soot-vapourization laser on as "SP-AMS" data. The HR-AMS and SP-AMS data were analyzed according to standard techniques[24] with uncertainties estimated by a recently-developed method[25]. The data presented herein are relative mass spectra, and therefore required only m/z calibration. Our m/z calibration was performed using internal background ions, again following standard techniques, as discussed in more detail elsewhere.[26]

As discussed in the manuscript, no difference was found in the HR-AMS mass spectra of HFO-PM compared to distillate-fuel PM produced from diesel or marine gas oil, when vapourizing particles on a 873 K tungsten surface. We also compared the HR-AMS mass spectra of HFO-PM with those of a dual-vapourizer SP-AMS, which adds a 1064 nm particle vapourization laser prior to the tungsten-surface vapourizer. Also no difference was observed (Supplementary Figure 5) in this case. This result is unexpected, since tar brC in HFO-PM has been shown in this manuscript to absorb at 950 nm. However, in order to be detected by SP-AMS, tar brC must not only absorb at 1064 nm, but also remain in the laser for a sufficient amount of energy to be absorbed for vapourization. The fact that we have not observed a difference in the SP-AMS mass spectra demonstrates that these conditions were not met by our sample. However, it may be possible to detect other tar brC samples, since a continuum of absorption efficiencies can be expected for tar brC in general, as discussed in the manuscript.

Absence of char in SEM images and elemental composition of SEM-identified tar brC

As noted in the manuscript, we observed the absence of char particles in our samples using SEM. We emphasize that our manual SEM analysis naturally focussed on larger particles, and zero char particles were identified. To add to the statistical power of this observation, we acquired low-magnification SEM micrographs and used image analysis to extract the sizes of 50,268 particles in terms of the major and minor axes of a fitted ellipse (Supplementary Figure 3**a,b**). With reference to the major axis of the fitted ellipses, the majority of the measured particles were smaller than 600 nm, with a count median diameter (CMD) around 200 nm, indicating the absence of a substantial number of char particles, as char particles have a characteristic diameter of 1 μm[11]. We note that the 200 nm mode may be biased high due to the high detection limit of this technique (not quantified). We also note that the absence of char BC in our samples does not mean that no char was formed in the engine, as char may have formed and been subsequently oxidized before emission (as is the case for the majority of soot BC mass[27]).

We were not able to measure the elemental composition of the tar brC identified by SEM, due to interference from carbon in the polycarbonate filter supporting the particles. Previous work has reported tar to consist mostly of carbon with some oxygen or nitrogen impurities, depending on the sample. Tivanski et al.[28] reported tar brC from wildfires to have an average O/C ratio of 0.8; Chakrabarty et al.[13] reported tar brC from from smouldering duff combustion to have an average O/C ratio of 0.17; and Alexander et al.[14] reported tar brC from an unknown source (hypothesized herein to be HFO combustion) to have a typical O/C ratio of 0.04, substantially lower than the other studies. Alexander et al.[14] also reported the N/C ratio of tar brC as 0.06.

Supplementary Figures 3**c**–**f** shows SEM images of various particle types identified in our samples. The particle types include soot-BC (Supplementary Figure 3**f**, smaller aggregates), inorganic ash (**c,d**), and tar (**e,f**). These classifications have been made according to particle morphology as follows. Soot BC was evident as being composed of aggregates of carbonaceous monomers. Tar brC particles were carbonaceous spheres (containing negligible amounts of elements other than carbon, oxygen and hydrogen according to electron dispersion spectroscopy measurements) and were involatile under the SEM vacuum and stable under the electron beam. Some tar brC was were internally mixed with soot or appeared to be associated with a film. That film likely reflects the volatile fraction of the PM sample, which for these samples likely consisted of sulfuric acid[26] and lubrication-oil-related OM[26,29], according to previous results from this same measurement campaign. While we could not quantify the number fraction of internally-mixed tar brC using our measurements, we could quantify the corresponding number of internally-mixed soot BC particles, as reported in a previous publication[26]. As this number fraction was negligible for soot BC, we assume it was also negligible for tar brC. The black circles in the figure are pores in the polycarbonate filter and the brighter entities are particles. Samples were covered with a 15nm thick Au film, evaporated in vacuum, in order to avoid charging of the sample under the electron beam.

Positive artifact in EC quantification for HFO-PM and asphaltenes

During thermal–optical analysis (TOA), some OC (that is, carbonaceous material other than BC[30]) may pyrolyze rather than volatilize at the oxygen-free stage, at some temperature below its vapourization temperature. Pyrolysis typically produces light-absorbing, thermally-refractory carbonaceous PM. To account for carbon "lost" to pyrolysis, the transmittance (or reflectance) of the sample is monitoring during TOA. Any decrease in transmittance (or reflectance) is ascribed to the formation of pyrolytic material. Following the addition of oxygen, the transmittance increases until all carbon is removed from the filter. The standard TOA analysis only assigns carbon to "EC" after the transmittance returns to its initial value (the so-called split point), the carbon evolved in oxygen prior to this return is labelled "pyrolyzed carbon" and assigned to OC.

Aside from the substantial uncertainty introduced when determining the split point in the presence of a continuously changing carbon signal, and a transmittance (or reflectance) signal which is influenced by instrument temperature, there are fundamental unknowns in the pyrolyzed-carbon assignment procedure. As clearly discussed by Yang and Yu[31], TOA requires that pyrolyzed carbon evolve at lower temperatures than EC, or have the same mass absorption efficiency as EC. Following from the tar-formation discussion in the main manuscript, the latter requirement is clearly unreasonable, as demonstrated by Yang and Yu[31] experimentally. Yang and Yu[31] also observed that the former requirement is not met for many sample types. Our asphaltene thermogram (Supplementary Figure 6**d**) also clearly shows that the pyrolyzed carbon (or pre-existing refractory carbon) in HFO asphaltenes does not evolve before true EC (which is expected to be chemically equivalent to BC) evolves (compare with the thermogram of diesel PM in Supplementary Figure 6**c**).

The inability of TOA to separate pyrolyzed carbon from true EC has two implications for the present study. First, pyrolysis corrections as described above cannot be relied upon. Second, if the small degree of pyrolysis which occurs in the TOA instrument for HFO asphaltenes allows refractory OC to form, then certainly the higher-temperature pyrolysis of HFO which forms tar within the engine will produce refractory material. Thus, our observation of HFO asphaltenes evolving during the EC stage of the thermogram indicates that tar brC will also evolve as apparent EC.

Finally, we note that at the "EC" stage, the asphaltene thermogram shows a broad peak of evolved carbon (Supplementary Figure 6**c**), clearly different to the peak seen for HFO-PM (Supplementary Figure 6**a**) or even diesel PM (Supplementary Figure 6**d**). It is tempting to interpret this difference as due to a chemical difference between asphaltenes and HFO-PM.

However, it may also be due to the fact that our asphaltene sample was deposited as a macroscopic solution droplet, and not as nanoscopic aerosol particles.

Independence of absorption by unburnt HFO on concentration

As noted in the Methods section of the main text, we measured the spectral absorption of unburnt HFO at multiple different concentrations, ranging from 4 mg/L to 100 mg/L. These measurements were motivated largely by debate within the crude-oil community as to the possibility of asphaltenes forming molecular aggregates, which have been postulated as the species responsible for the usually high absorption of asphaltenes in the near infrared[32]. The formation of molecular aggregates would be concentration dependent, so our measurements of the independence of absorption with concentration provide evidence against this effect. Moreover, a number of independent lines of experimental evidence have also demonstrated that this effect not the most likely reason for the infrared-absorbing property of asphaltenes, as discussed in detail by Mullins[32].

Implications for the interpretation of previous HFO-PM results

We have previously published a manuscript[26] where we retrieved imaginary refractive indices k_{OM} for HFO-PM brC by combining absorption coefficient measurements with OM mass concentration measurements taken with an AMS. By assuming an AAE of unity for BC, and attributing all near-infrared light absorption to BC, we reported k_{OM} and MAC_{OM} as a function of engine load. It was noted in that manuscript that the above calculation, referred to as the two-component BC+brC model, may not fully describe HFO-PM due to the possible presence of asphaltenes and char BC. It was also noted that such a model need not fully describe the aerosol to be useful, as climate models which combine OC emission factors with Mie theory to predict aerosol properties may still benefit from the reported k_{OM} values. These conclusions remain true and the k_{OM} provided in Corbin et al.[26] remain valid. However, the present identification of tar brC as the key brC species in HFO-PM means that OM concentrations (which do not include tar) are not the most appropriate factor by which to normalize brC absorption. Future studies should directly quantify and normalize to tar brC concentrations, for example by combining rBC with EC measurements as done in the present study. Additionally, the solvent-extraction results in the present manuscript demonstrate that the presence of asphaltenes was not a source of uncertainty in the two-component BC+brC model; rather, tar brC was.

The emission factors reported by Corbin et al.[26] were calculated in terms of rBC and OM, along with apparent imaginary refractive indices for OM (by combining the rBC and OM data with calibrated light-absorption measurements). According to the present manuscript, those results could be recast in terms of soot BC and tar brC absorption. Alternatively, the results could be reported in terms of wavelength-resolved absorption coefficients $b(\lambda)$. (equivalent to wavelength-resolved eBC, but without including the assumption of a MAE). We have chosen the latter option, and report here the emission factors from Corbin et al.[26] in terms of $b(\lambda)$, to avoid propagating the uncertainties associated with dividing absorption into soot BC and tar brC into the results. The new emission factors are available online as a supplementary file.

In addition, another manuscript has been published using data from the present study[33]. None of the conclusions of that study are influenced by the present work, as that work focussed on metals in soot BC measured by SP-AMS. The present work has confirmed that tar brC is not a confounding species for the SP-AMS detection of soot BC.

2 Supplementary Figures

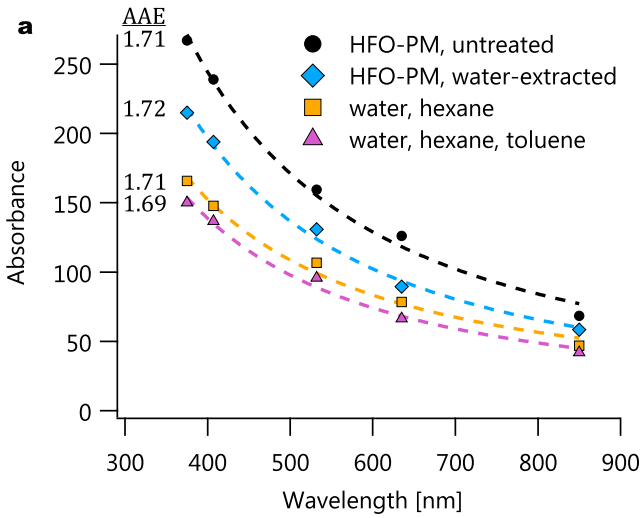

Supplementary Figure 1. Spectral absorbance measured by MWAA, corresponding to Figure 2**a**. The labelled AAEs are the AAE(375,850). The slight decrease in absolute absorbance due to water extraction is attributed to the removal of sulfates[26] and the decrease due to hexane is attributed to the removal of lubrication-oil PM[29] from the filters. Although these PM components do not absorb visible light, they may influence total absorbance by scattering light towards LAC particles. It is very unlikely that these reductions reflect the removal of soluble brC, since the AAE of smaller and more-soluble brC molecules would be expected to be significantly higher than that of larger, insoluble brC[23].

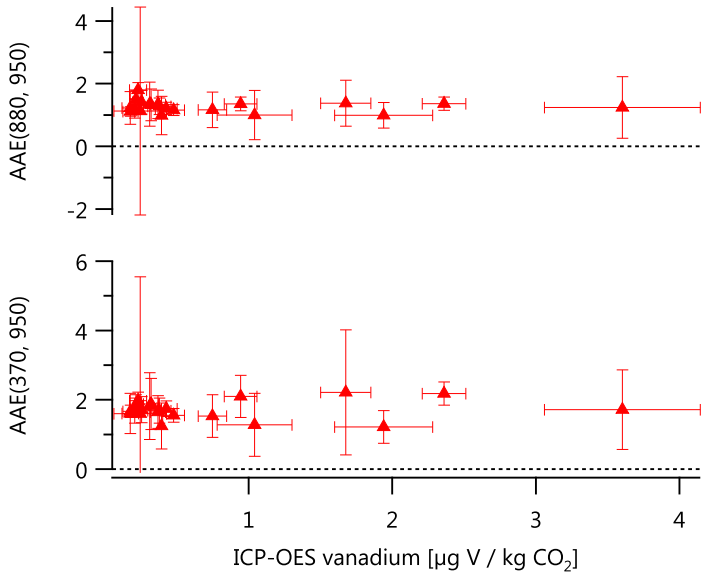

Supplementary Figure 2. Vanadium emission factors varied widely between conditions, and did not correlate with the AAE. Vanadium-related absorption (eg, from VO_2) is therefore unlikely to have influenced the discussion in this manuscript. These vanadium data were acquired using an inductively-coupled plasma optical-emission spectrometer (ICP-OES) as part of this study and have been described in Corbin et al.[33]. Note that the data of Corbin et al.[33] suggest that the chemical state of the vanadium was similar in all cases. Error bars for the AAEs are standard error of the mean, for the ICP-OES data are the sum in quadrature of the standard deviation of the background signal and 5% of the measured signal[33].

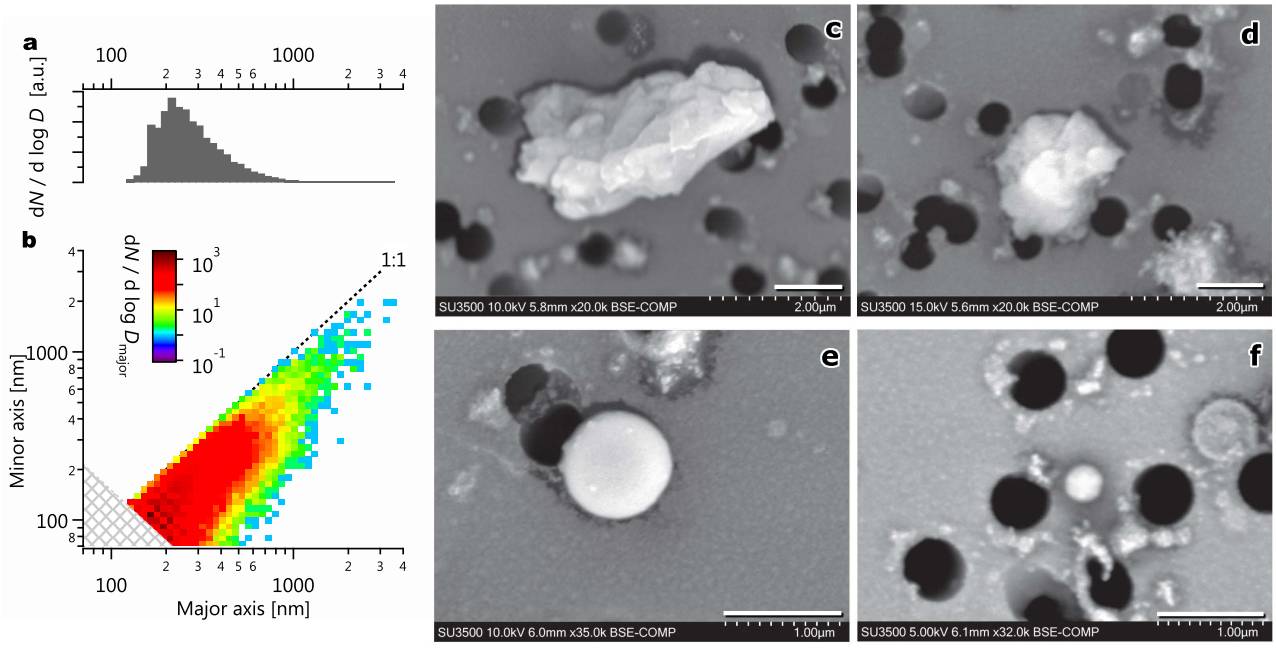

Supplementary Figure 3. Micrographs and sizes of HFO-PM particles analyzed by SEM. (**a,b**) 1D and 2D size distributions of 50,268 particles, in terms of the major and minor diameters of an equivalent ellipse. The sharp cutoff at lower sizes (grey cross-hatching) reflects an area limit of detection of 0.05 μm^2. Dust particles (**c,d**), soot-BC (**f**, smaller aggregates), and (**ef**) tar brC spheres are seen in the micrographs. Note the varying size of the white scale bars, each of which is 1 μm. The numerous black circles are holes in the polycarbonate filter.

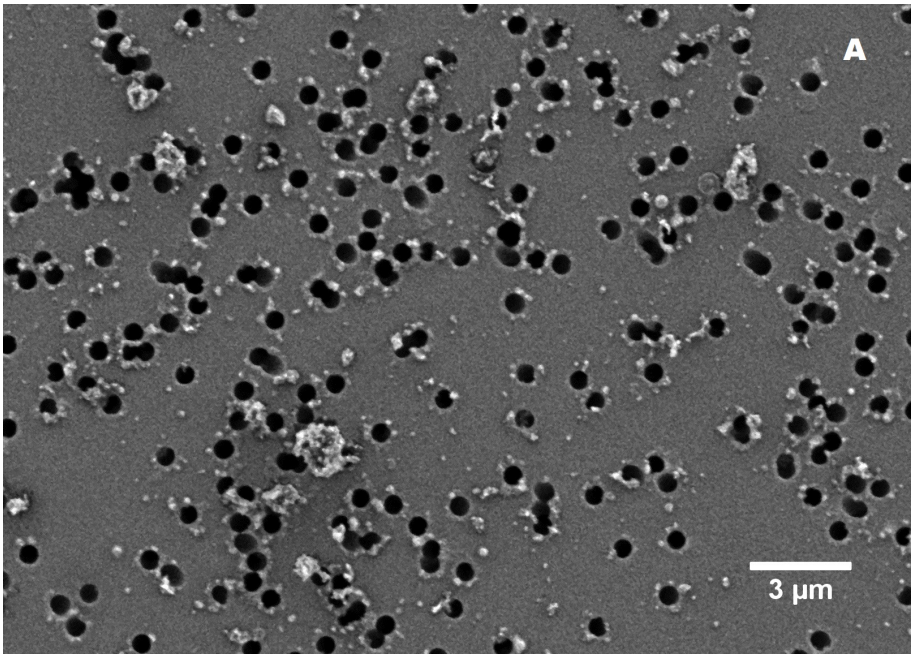

Supplementary Figure 4. (**A**) Low-magnification secondary-electron SEM image of an HFO PM filter sample, taken at 3 kV accelerating voltage. Black circles indicate holes in the polycarbonate filter. Multiple soot aggregates are visible.

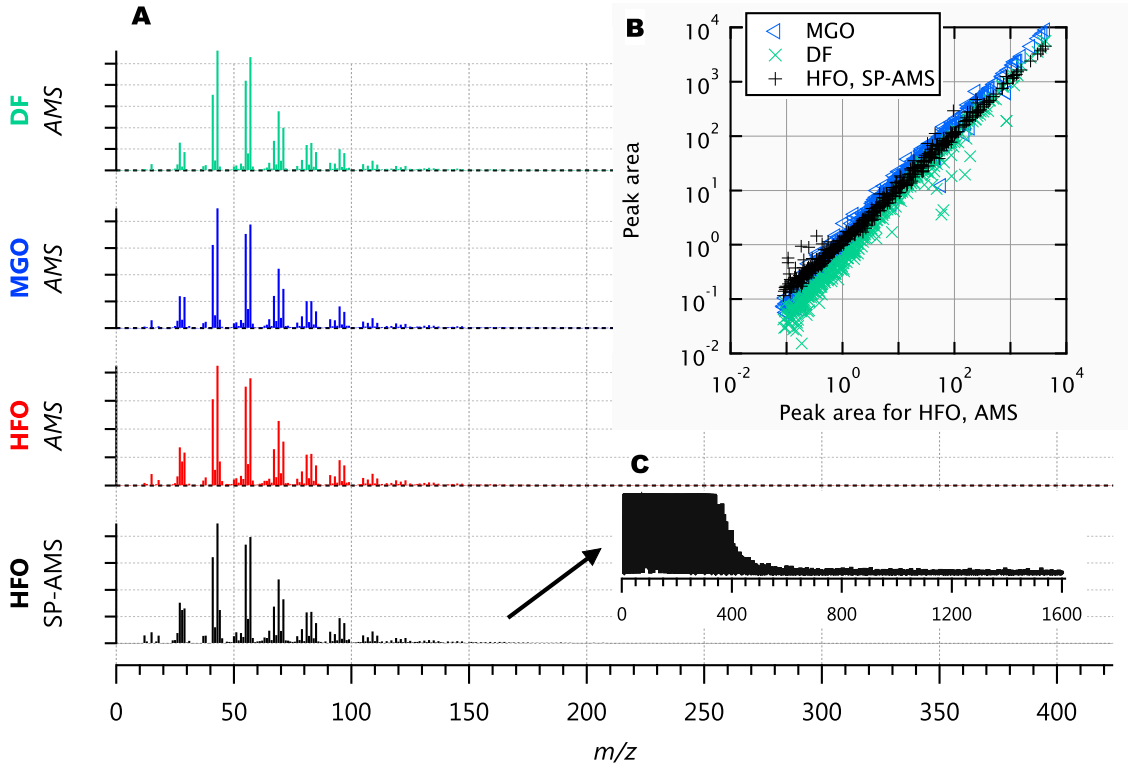

Supplementary Figure 5.
A. AMS and SP-AMS organic mass spectra of all three fuels (heavy fuel oil HFO, marine gas oil MGO, diesel fuel DF). Sulfate-related ions have been omitted. The spectra appear equivalent, even though the OM mass absorption cross section varied[26], suggesting a lubrication-oil source, consistent with the conclusions of Ref.[29]. The similarity of the SP-AMS and AMS mass spectra indicate that the majority of the vaporized material was vapourized by the AMS vapourizer (that is, non-1064-nm light absorbing). The OM elemental ratios were H:C= 1.87, O:C=0.02 and the corresponding OM:OC ratio was 1.20 (Ref[33]). **B.** Scatterplots of each mass spectrum in **A** with the HFO AMS mass spectrum. **C.** Zoom in of the SP-AMS HFO mass spectrum scatterplot showing negligible high-mass aromatic or carbon-cluster signals (no background subtraction or peak integration was performed).

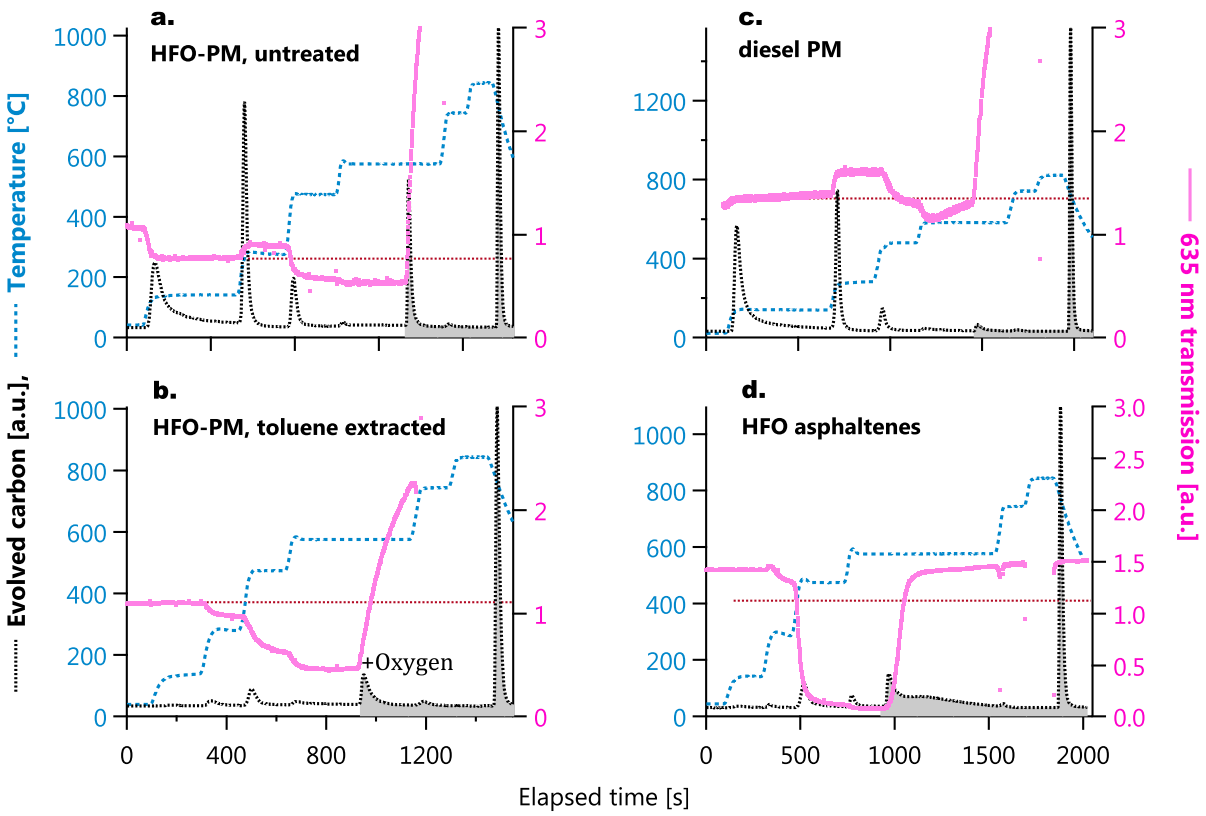

Supplementary Figure 6. Thermal–optical analyses (IMPROVE-A protocol) of **(a)** HFO PM, **(b)** toluene-extracted HFO-PM (same filter as Fig. 2), **(c)** diesel PM, **(d)** the asphaltene fraction of our HFO sample (ASTM protocol). Black dotted lines show evolved carbon and blue dashed lines the sample temperature. Pink dots (right axis) show the filter transmittance at 635 nm. Grey shading indicates the addition of oxygen. Each run ends with a methane spike for detector calibration. The near-complete disappearance of OC1 and OC2 signals after to solvent extraction shows that soluble OC was also volatilizable OC. (OC3 and OC4 cannot be included in this evaluation due to their association with pyrolytically-produced compounds[34]).

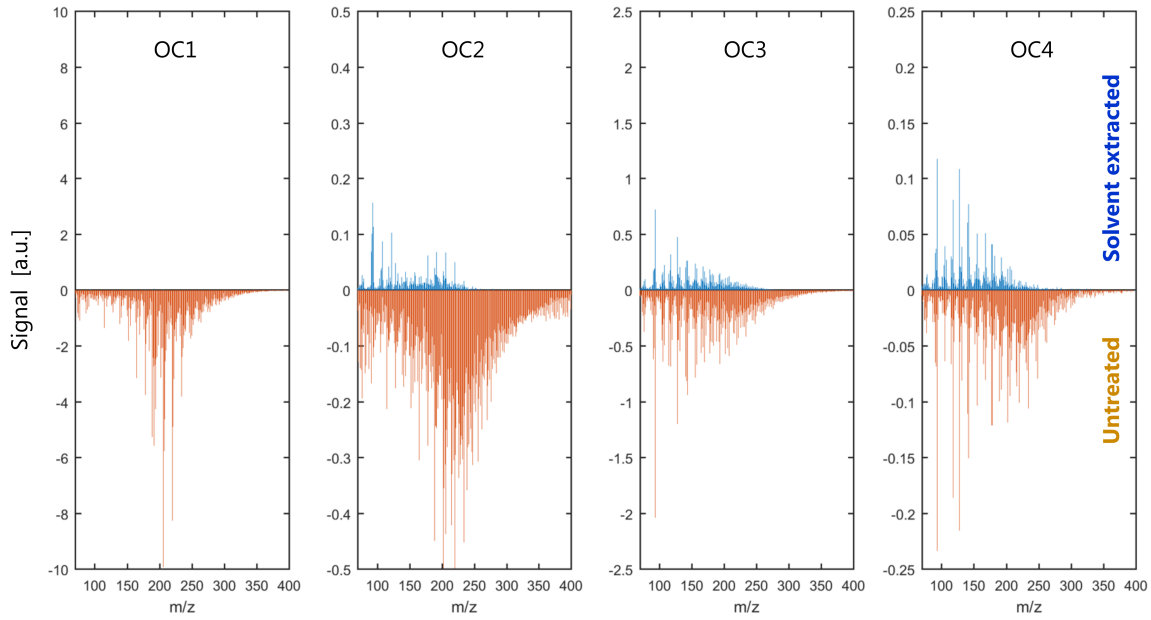

Supplementary Figure 7. Resonance-enhanced multiphoton ionization (REMPI) mass spectra obtained during the TOA analysis of untreated and solvent-extracted HFO-PM filters. Note that the appearance of lower-m/z peaks during the OC3 and OC4 stages is indicative of pyrolysis-generated aromatics.

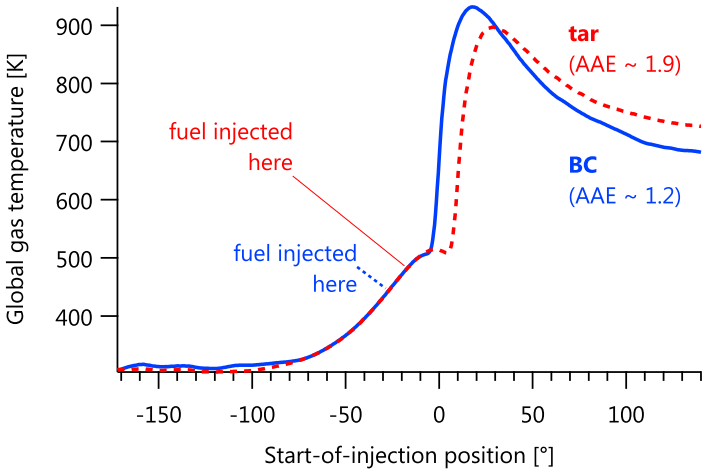

Supplementary Figure 8. Global gas temperature calculated using a zero-dimensional thermodynamic model of the engine. Under conditions where tar-like PM was produced (red dashed line, labelled "tar"), injected fuel is predicted to have spent a longer time at moderate temperature ($\sim$ 500 K) prior to ignition, and to have reached a lower absolute temperature, relative to conditions where BC-like PM was produced (blue solid line, labelled "BC").

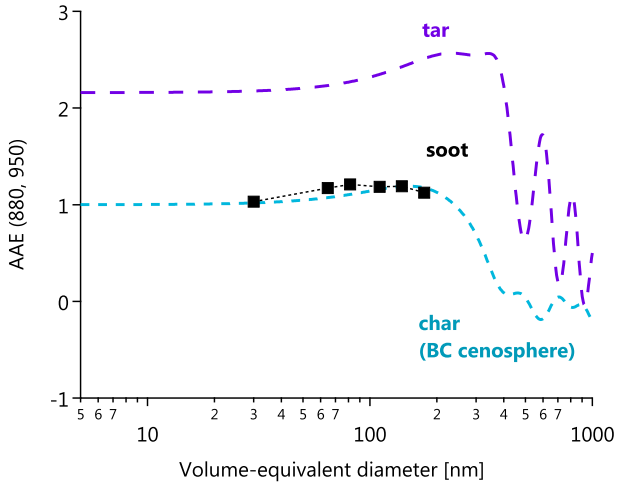

Supplementary Figure 9. Theoretical AAE(880nm,950nm) for LAC as a function of size, including tar, soot-BC, and char-BC cenospheres.

Supplementary References

1. Schwarz, J. P. *et al.* Single-particle measurements of midlatitude black carbon and light-scattering aerosols from the boundary layer to the lower stratosphere. *J. Geophys. Res.* **111**, D16207 (2006). DOI 10.1029/2006JD007076.

2. Petzold, A. *et al.* Recommendations for the interpretation of "black carbon" measurements. *Atmos. Chem. Phys.* **13**, 8365–8379 (2013). DOI 10.5194/acp-13-8365-2013.

3. Bond, T. C. *et al.* Bounding the role of black carbon in the climate system: A scientific assessment. *J. Geophys. Res. Atmos.* **118**, 5380–5552 (2013). DOI 10.1002/jgrd.50171.

4. Lack, D. A. *et al.* Brown carbon and internal mixing in biomass burning particles. *Proc. Natl. Acad. Sci.* **109**, 14802–14807 (2012). DOI 10.1073/pnas.1206575109.

5. Saleh, R. *et al.* Brownness of organics in aerosols from biomass burning linked to their black carbon content. *Nat. Geosci.* **7**, 647–650 (2014). DOI 10.1038/ngeo2220.

6. Laskin, A., Laskin, J. & Nizkorodov, S. A. Chemistry of atmospheric brown carbon. *Chem. Rev.* **115**, 4335–4382 (2015). DOI 10.1021/cr5006167.

7. Lobo, P. *et al.* Measurement of aircraft engine non-volatile pm emissions: Results of the aviation-particle regulatory instrument demonstration experiment (a-pride) 4 campaign. *Aerosol Sci. Technol.* **0**, 00–00 (2015). DOI 10.1080/02786826.2015.1047012.

8. Torvela, T. *et al.* Effect of wood combustion conditions on the morphology of freshly emitted fine particles. *Atmos. Environ.* **87**, 65–76 (2014). DOI 10.1016/j.atmosenv.2014.01.028.

9. Schmidt, M. W. I. & Noack, A. G. Black carbon in soils and sediments: Analysis, distribution, implications, and current challenges. *Glob. Biogeochem. Cycles* **14**, 777–793 (2000). DOI 10.1029/1999gb001208.

10. Linak, W. P., Miller, C. A. & Wendt, J. O. Fine particle emissions from residual fuel oil combustion: Characterization and mechanisms of formation. *Proc. Combust. Inst.* **28**, 2651–2658 (2000). DOI 10.1016/s0082-0784(00)80684-0.

11. Chen, Y., Shah, N., Braun, A., Huggins, F. E. & Huffman, G. P. Electron microscopy investigation of carbonaceous particulate matter generated by combustion of fossil fuels. *Energy & Fuels* **19**, 1644–1651 (2005). DOI 10.1021/ef049736y.

12. Elmquist, M., Cornelissen, G., Kukulska, Z. & Örjan Gustafsson. Distinct oxidative stabilities of char versus soot black carbon: Implications for quantification and environmental recalcitrance. *Glob. Biogeochem. Cycles* **20**, n/a–n/a (2006). DOI 10.1029/2005gb002629.

13. Chakrabarty, R. *et al.* Brown carbon in tar balls from smoldering biomass combustion. *Atmos. Chem. Phys.* **10**, 6363–6370 (2010). DOI doi:10.5194/acp-10-6363-2010.

14. Alexander, D. T. L., Crozier, P. A. & Anderson, J. R. Brown carbon spheres in east asian outflow and their optical properties. *Sci.* **321**, 833–836 (2008). DOI 10.1126/science.1155296.

15. Seinfeld, J. H. & Pandis, S. N. *Atmospheric chemistry and physics: from air pollution to climate change* (John Wiley & Sons, 2012).

16. Bond, T. C. & Bergstrom, R. W. Light absorption by carbonaceous particles: An investigative review. *Aerosol Sci. Technol.* **40**, 27–67 (2006). DOI 10.1080/02786820500421521.

17. Sun, H., Biedermann, L. & Bond, T. C. Color of brown carbon: A model for ultraviolet and visible light absorption by organic carbon aerosol. *Geophys. Res. Lett.* **34** (2007). DOI 10.1029/2007gl029797.

18. Moschos, V. *et al.* Source apportionment of brown carbon absorption by coupling ultraviolet–visible spectroscopy with aerosol mass spectrometry. *Environ. Sci. & Technol. Lett.* **5**, 302–308 (2018). DOI 10.1021/acs.estlett.8b00118.

19. Kumar, N. K. *et al.* Production of particulate brown carbon during atmospheric aging of residential wood-burning emissions. *Atmospheric Chem. Phys.* **18**, 17843–17861 (2018). DOI 10.5194/acp-18-17843-2018.

20. Scarnato, B., Vahidinia, S., Richard, D. & Kirchstetter, T. Effects of internal mixing and aggregate morphology on optical properties of black carbon using a discrete dipole approximation model. *Atmos. Chem. Phys.* **13**, 5089–5101 (2013). DOI 10.5194/acp-13-5089-2013.

21. Hoffer, A., Tóth, A., Nyirő-Kósa, I., Pósfai, M. & Gelencsér, A. Light absorption properties of laboratory-generated tar ball particles. *Atmos. Chem. Phys.* **16**, 239–246 (2016). DOI 10.5194/acp-16-239-2016.

22. Lu, Z. *et al.* Light absorption properties and radiative effects of primary organic aerosol emissions. *Environ. Sci. Technol.* **49**, 4868–4877 (2015). DOI 10.1021/acs.est.5b00211.

23. Saleh, R., Cheng, Z. & Atwi, K. The brown–black continuum of light-absorbing combustion aerosols. *Environ. Sci. & Technol. Lett.* (2018). DOI 10.1021/acs.estlett.8b00305.

24. Sueper, D., Jimenez, J. L., Aiken, A. & DeCarlo, P. Pika tof-ams high resolution analysis software (2011). URL `cires.colorado.edu/jimenez-group/ToFAMSResources/ToFSoftware/PikaInfo`. Last accessed October 2015.

25. Corbin, J. C. *et al.* Peak-fitting and integration imprecision in the aerodyne aerosol mass spectrometer: effects of mass accuracy on location-constrained fits. *Atmos. Meas. Tech.* **8**, 4615–4636 (2015). DOI 10.5194/amt-8-4615-2015.

26. Corbin, J. C. *et al.* Brown and black carbon emitted by a marine engine operated on heavy fuel oil and distillate fuels: optical properties, size distributions, emission factors. *J. Geophys. Res. Atmospheres* **123**, 6175–6195 (2018). DOI 10.1029/2017JD027818.

27. Glassman, I. & Yetter, R. A. *Combustion* (Academic Press, Burlington, MA, USA, 2008).

28. Tivanski, A. V., Hopkins, R. J., Tyliszczak, T. & Gilles, M. K. Oxygenated interface on biomass burn tar balls determined by single particle scanning transmission x-ray microscopy. *J. Phys. Chem. A* **111**, 5448–5458 (2007). DOI 10.1021/jp070155u.

29. Eichler, P. *et al.* Lubricating oil as a major constituent of ship exhaust particles. *Environ. Sci. Technol. Let.* **4**, 54–58 (2017). DOI 10.1021/acs.estlett.6b00488.

30. Pöschl, U. Atmospheric aerosols: Composition, transformation, climate and health effects. *Angewandte Chemie Int. Ed.* **44**, 7520–7540 (2005). DOI 10.1002/anie.200501122.

31. Yang, H. & Yu, J. Z. Uncertainties in charring correction in the analysis of elemental and organic carbon in atmospheric particles by thermal/optical methods. *Environ. Sci. & Technol.* **36**, 5199–5204 (2002). DOI 10.1021/es025672z.

32. Mullins, O. C. The modified yen model. *Energy & Fuels* **24**, 2179–2207 (2010). DOI 10.1021/ef900975e.

33. Corbin, J. C. *et al.* Trace metals in soot and $pm_{2.5}$ from heavy-fuel-oil combustion in a marine engine. *Environ Sci Technol* (2018). DOI 10.1021/acs.est.8b01764.

34. Streibel, T. *et al.* Aerosol emissions of a ship diesel engine operated with diesel fuel or heavy fuel oil. *Environ. Sci. Pollut. Res.* 10976 (2017). DOI 10.1007/s11356-016-6724-z.